iScience

CellPress
OPEN ACCESS

Article

Dynamic Neuroimmune Profile during Mid-life Aging in the Female Brain and Implications for Alzheimer Risk

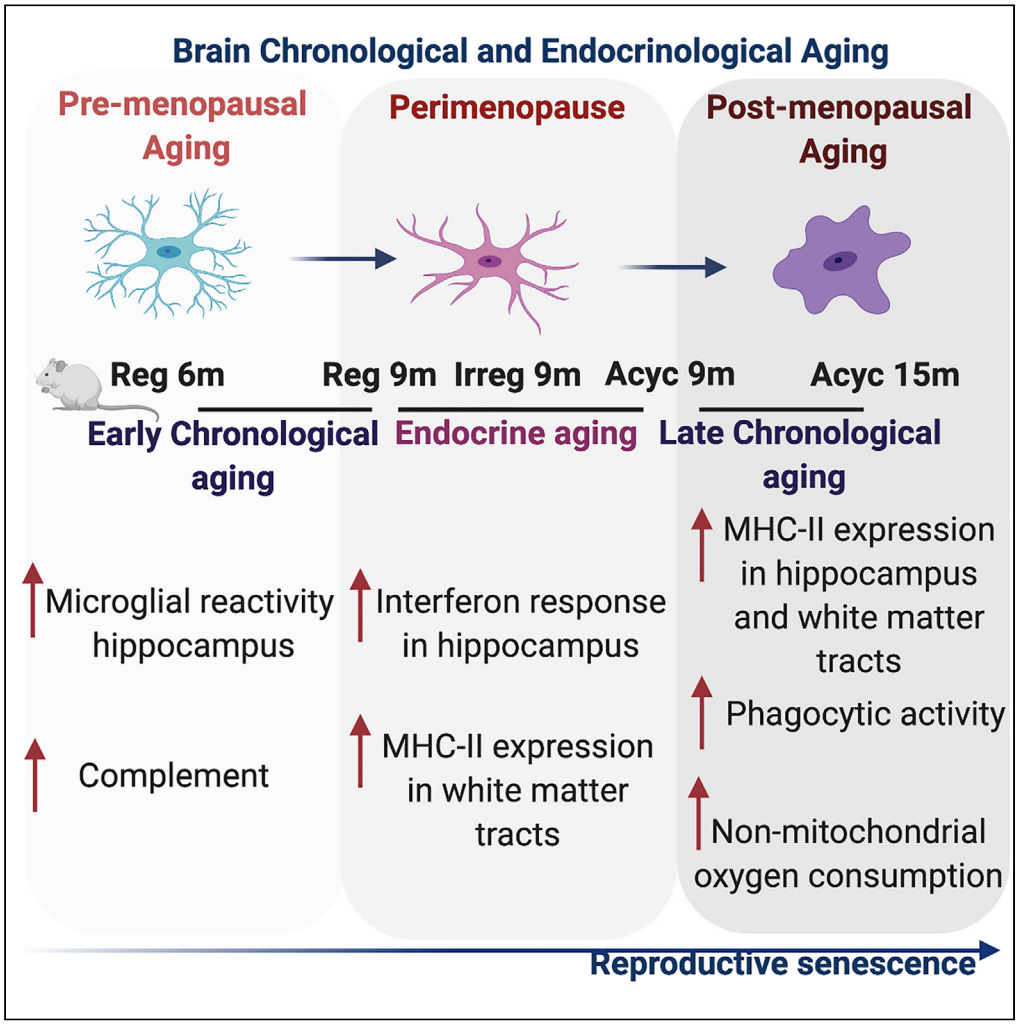

Aarti Mishra, Yuan Shang, Yiwei Wang, Eliza R. Bacon, Fei Yin, Roberta D. Brinton

rbrinton@arizona.edu

HIGHLIGHTS

Neuroimmune profile was dynamic across aging transitions in female brain

Microglial reactivity was spatially dependent and most evident in white matter

Neuroimmune signature of perimenopause parallels neurodegenerative profile

Discovery outcomes profiles human hippocampal immune microarray profile in women

Mishra et al., iScience 23, 101829
December 18, 2020
https://doi.org/10.1016/j.isci.2020.101829

iScience

CellPress
OPEN ACCESS

Article

Dynamic Neuroimmune Profile during Mid-life Aging in the Female Brain and Implications for Alzheimer Risk

Aarti Mishra,[1] Yuan Shang,[1] Yiwei Wang,[1] Eliza R. Bacon,[2] Fei Yin,[1] and Roberta D. Brinton[1,3,*]

SUMMARY

Aging and endocrine transition states can significantly impact inflammation across organ systems. Neuroinflammation is well documented in Alzheimer disease (AD). Herein, we investigated neuroinflammation that emerges during mid-life aging, chronological and endocrinological, in the female brain as an early initiating mechanism driving AD risk later in life. Analyses were conducted in a translational rodent model of mid-life chronological and endocrinological aging followed by validation in transcriptomic profiles from women versus age-matched men. In the translational model, the neuroinflammatory profile of mid-life aging in females was endocrine and chronological state specific, dynamic, anatomically distributed, and persistent. Microarray dataset analyses of aging human hippocampus indicated a sex difference in neuroinflammatory profile in which women exhibited a profile comparable to the pattern discovered in our translational rodent model, whereas age-matched men exhibited a profile consistent with low neuroimmune activation. Translationally, these findings have implications for therapeutic interventions during mid-life to decrease late-onset AD risk.

INTRODUCTION

Neuroinflammatory processes are at the core of the dysregulated pathophysiology observed in Alzheimer's disease (AD) (Akiyama et al., 2000; Eikelenboom et al., 1994; Griffin, 2006; Heneka et al., 2015; Itagaki et al., 1989; Mattiace et al., 1990; McGeer et al., 1987, 1989; Van Eldik et al., 2016). Yet, the inflammatory processes by which pathophysiology of AD is promoted and their contribution to the prodromal phase of late-onset AD remains to be fully understood.

The systems biology of immune response is dynamic and changes in concert with disease progression (Mishra and Brinton, 2018). Inflammation increases with age, in the brain and periphery (Chung et al., 2019; Lynch, 2010; Sanada et al., 2018; Simen et al., 2011). Although the increase in inflammation is evident in both females and males, the trajectories undertaken are different (Da Silva, 1995; Gubbels Bupp et al., 2018; Klein and Flanagan, 2016; Márquez et al., 2020; McCruden and Stimson, 1991; Roved et al., 2017; Ruggieri et al., 2018). Sex differences in immunity during aging have been well documented in peripheral immune cells (Klein and Flanagan, 2016; Márquez et al., 2020). Females experience an increase in inflammation during the perimenopausal transition, which is marked by an increase in peripheral CD4/CD8 T cell ratio, number of CD4 T cells and B cells, and cytokine levels—interferon (IFN)-γ, interleukin (IL)-6, and IL-8 (Klein and Flanagan, 2016; Mishra and Brinton, 2018; Straub, 2007). Much like in the periphery, menopause is associated with an increase in inflammation in brain (Mishra and Brinton, 2018; Sárvári et al., 2012, 2014; Sohrabji, 2007; Yin et al., 2015). Loss of ovarian hormones causes increased expression of microglial reactivity markers linked to interaction with T cells in the hippocampus and frontal cortex (Sárvári et al., 2012, 2014).

Sex-specific transitions in brain metabolism are apparent early in mid-life aging, which are coincident with endocrine transition of peri-to-post menopause (Brinton et al., 2015), and can be a tipping point in neurological aging (Brinton et al., 2015). The perimenopausal transition in females is marked by a bioenergetic deficit characterized by reduced glucose metabolism in brain as detected by 2-deoxy-2-[^{18}F]fluoro-d-glucose positron emission tomography (^{18}F-FDG-PET) and concomitant downregulation of glucose

[1]Center for Innovation in Brain Science, University of Arizona, Tucson, AZ 85719, USA

[2]Department of Medical Oncology, Beckman Research Institute, City of Hope, Duarte, CA 91010, USA

[3]Lead Contact

*Correspondence: rbrinton@arizona.edu

https://doi.org/10.1016/j.isci.2020.101829

transporter 3 (GLUT3), pyruvate dehydrogenase 1 (PDH1), and oxidative phosphorylation (Ding et al., 2013a, 2013b; Yao and Brinton, 2012; Yao et al., 2012; Yin et al., 2015). Sex-differences in the bioenergetic trajectory of aging are apparent in both mechanistic and clinical analyses (Mosconi et al., 2017b, 2018; Yin et al., 2015; Zhao et al., 2016). Metabolic decline in the brain is an early indicator of the prodromal phase of AD and can be an initiator of chronic inflammation, which is involved in the pathophysiology of the disease (Wang et al., 2020; Yin et al., 2015, 2016). The greater prevalence of AD in women is often attributed to the 4.5 years of greater life span in women (Association, 2018; Nebel et al., 2018; Niu et al., 2017); however, midlife deficits in glucose metabolism and activation of inflammatory processes could be early indicators of prodromal AD contributing to the sex difference in AD prevalence.

To address the role of the neuroimmune system in mechanisms underlying AD in the female, we hypothesized that the mid-life endocrine aging transition in the female initiates neuroinflammation in the brain. To investigate the effect of each chronological and endocrinological aging phase on the neuroinflammatory phenotype, we conducted analyses in the perimenopausal animal model that mimics the perimenopausal transition in its emergence of reproductive irregularity followed by acyclicity (Yin et al., 2015; Bacon et al., 2019; Wang et al., 2020).

Using bulk RNA-Seq of the hippocampus, we investigated inflammatory pathways that are regulated during chronological and endocrine aging windows. Outcomes of these analyses indicated a neuroinflammatory phenotype that dynamically changes during female midlife aging involving a spectrum of glial phenotypes. Spatial mapping of major histocompatibility complex class II (MHC-II), a microglial reactivity marker, revealed increased immunoreactivity in white matter tracts: cingulum, corpus callosum, and fimbria during mid-endocrine aging phase. In parallel, microglial cells exhibited decreased phagocytic capacity. Dynamic changes in the immune profile were paralleled by glial-cell-specific alterations in mitochondrial function. Microglia exhibited a shift toward non-mitochondrial respiration, whereas astrocytes exhibited an increase in mitochondrial spare and maximal respiration. Estradiol administered immediately following ovariectomy prevented transition to an inflammatory profile, whereas estradiol administered weeks following ovariectomy was partially effective.

To address the translational validity of these findings, microarray data from mid-life human female and male hippocampi were analyzed. A sex difference in neuroinflammatory profile was evident in which women exhibited a profile comparable to the pattern discovered in our translational rodent model, whereas age-matched men exhibited a profile consistent with low neuroimmune activation. As in the translational model, the neuroinflammatory profile in women was dynamic, anatomically distributed, and persistent. Collectively, these findings provide a foundation upon which to create a precision therapeutic strategy to prevent, delay, or treat neuroinflammation as an initiating and accelerating driver of Alzheimer risk in women.

RESULTS

Hippocampal Neuroinflammatory Transcriptomic Profile Is Chronological Aging and Endocrinological Aging Specific

To interrogate a broad immune systems biology, an unbiased transcriptomic analysis was conducted. Transcriptomic profiling conducted by bulk RNA-Seq of the hippocampus during chronological and endocrinological aging revealed that genes involved in neuroinflammation were significantly affected during the course of chronological and endocrinological aging, in comparison to regular cycling 6-month-old (Reg 6m) (Figure 1 and Table S1). Further, each stage of the aging window exhibited a unique profile. Upregulation of *Apoe*, *Trem2*, *Tyrobp*, a gene expression signature that has recently been implicated with a disease-associated microglia (DAM) phenotype (Keren-Shaul et al., 2017), was evident in the chronological aging phase that precedes the onset of perimenopause, (Reg 9m versus Reg 6m) (Figure 1). Co-incident with the expression of DAM genes was an upregulation of complement genes, and microglial reactivity including *Cd68*, *Aif1*, *Fscn1*, *Tgfa*, and MHC-I and -II (*Rt1-A1*, *Rt1-Dmb*). The *Cd200* gene that codes for a protein required for communication between microglia and neurons through *Cd200r* was significantly downregulated at onset of chronological aging (Reg 9m versus Reg 6m).The perimenopause (Irreg 9m versus Reg 6m) was uniquely characterized by downregulation of genes involved in transforming growth factor-β (TGF-β) signaling (*Mapk3*, *Nog*, *Tgfb3*), *Apoe*, *Trem2*, *Tyrobp*, and complement signaling (Figure 1). Interestingly, the perimenopause was characterized by upregulation in genes involved in lipid metabolism (*Abca1*, *Vegfa*, *Nos3*, *Ide*, *Pla2g10*) and type I and type II interferon response (*B2m*, *Irf4*, *Itgb7*, *Ifnar2*,

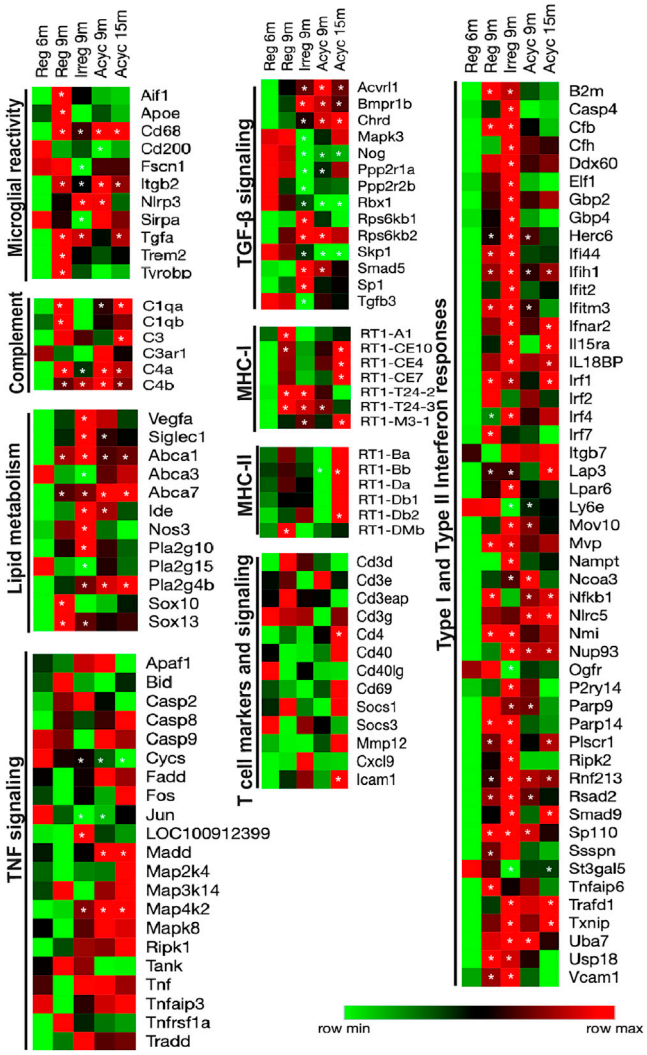

Figure 1. Transcriptomic Profiling of Endocrine and Chronological Aging (Early and Late) Female Rat Hippocampus

Heatmap visualization of hippocampal differential gene expression analysis of Reg 9m, Irreg 9m, Acyc 9m, and Acyc 15m with respect to Reg 6m, pathway analysis focused on microglial reactivity, complement, lipid metabolism, transforming growth factor β (TGF-β) signaling, major histocompatibility complex (MHC) class I and class II, tumor necrosis factor (TNF) signaling, type I and type II interferon signaling, and T cell markers and signaling. *p < 0.05 for differential gene expression analysis of the biological groups with respect to Reg 6m; calculated using student t-test. Detailed p-values and adjusted p values<0.05 for the differential gene expression analysis with respect to Reg 6m are listed in Table S1).

Txnip, *Usp18*) (Figure 1). The significant rise in the perimenopausal gene expression profile appeared to be initiated during the preceding chronological aging as evidenced by upregulation of *B2m*, *Irf1*, *Irf2*, and *Irf7* (Figure 1).

Transition into acyclicity and reproductive senescence (Acyc 9m) was marked by downregulation of type I and type II interferon responses and lipid metabolism (Figure 1). The Acyc 9m group was also characterized by an upregulation of gene expression of phospholipase *Pla2g4b*, lipid transport *Abca7*, and microglial lysosomal marker *Cd68*. Late-chronological aging post-menopause (Acyc 15m) was characterized by an upregulation of the MHC-II genes (*Rt1-Ba*, *Rt1-Bb*, *Rt1-Da*, *Rt1-Db1*, and *Rt1-Db2*) (Figure 1). Upregulation of genes involved in myelin breakdown, (*Pla2g4b*), lipid transport (*Abca7*), and lysosomal microglial marker (*Cd68*) was sustained into late chronological aging. Co-incident with this expression profile was an upregulation in genes involved in tumor necrosis factor (TNF) signaling and T helper cell marker *Cd4*.

Increased in *Cd4* expression was accompanied by increased T cell activation marker expression, *Cd69*, and adhesive molecule *Icam-1* (Figure 1). Validation was conducted by real-time quantitative PCR (RT-PCR). Consistent with RNAseq result, MHC-II expression was significantly increased in the Acyc 15m group (*Rt1-Ba fold change = 1.38*, *Rt1-Da fold change = 6.27*, and *Rt1-Db fold change = 9.56*, *with respect to Reg 6m control*).

Collectively, these data indicate that chronological pre-menopausal aging phase was characterized by up-regulation of DAM genes, whereas the endocrine peri-menopausal phase by type I and type II interferon response and the post-menopausal phase was marked by upregulation of MHC-II genes, indicating a dynamic shift in microglial reactivity. Collectively, these transcriptomic data are consistent with a dynamic trajectory in patterns of lipid metabolism and microglial gene expression predictive of a shift in neuroimmune transcriptome and functional phenotype.

Microglial Reactivity during Endocrine Aging Selectively Targeted White Matter

On the basis of transcriptomic evidence, the distribution of microglial reactivity was mapped in brain using the microglial marker, ionized calcium binding adaptor molecule (IBA-I, red), and MHC-II (green) microglial reactivity marker (Figures 2A–2E).

Spatial mapping of microglial reactivity across the brain revealed that white matter areas, corpus callosum, cingulum, and fimbria, exhibited increased microglial reactivity evidenced by elevated MHC-II positive microglia in early endocrine aging (Irreg 9m) (Figures 2A–2C and 2E) and in late chronological aging (Acyc 15m) (Figures 2B, 2C, and 2E). The hippocampus proper exhibited an increase in microglial reactivity in Irreg 9-month group, although to a lesser extent relative to the white matter (Figures 2D and 2E). Increased presence of microglial reactivity in white matter tracts is consistent with earlier findings (Klosinski et al., 2015) and indicate the potential for myelin catabolism as a source of ketone bodies to fuel energy demand of the brain (Klosinski et al., 2015).

Dynamics of Microglial Oxidative Stress, Phagocytosis, and Reactivity across Chronological and Endocrine Aging

During endocrine aging transitions upregulation of type I and type II interferon responses were coincident with increased microglial expression of MHC-II, a marker of reactivity in white matter. Based on this evidence, we hypothesized that microglial phagocytic function and associated free radical generation would be affected in the transition to reproductive senescence. To investigate this issue, single cell suspensions of pooled dissociated cortices, hippocampi, fimbria, and corpus callosum from each group were generated followed by flow cytometry detection of microglial mitochondrial free radical production, phagocytic capacity, and reactivity marker expression. Microglial cells were gated first for total cells (Figure 3A), followed by singlets (Figure 3B), followed by gating for CD11b (FITC) high and CD45 (VioBlue) intermediate (Figure 3C).

Microglial mitochondrial generation of reactive oxygen species (ROS) was assessed by measurement of MitoSOX positive microglial cells (Figure 3D). The uptake of MitoSOX was highest in the mid-endocrine aging (Irreg 9m) group (Figure 3G). Coincident with the increase in microglial cells contributing to mitochondrial ROS production was a reduction in microglia participating in phagocytosis (Figures 3E and 3H) evidenced by reduction in percentage of cells phagocytosing pHrodo *Staphylococcus aureus* Bioparticle conjugates (Figures 3E and 3H). Phagocytic capacity increased and reached maximum after late chronological aging (Acyc 12m group). Microglial reactivity marker—MHC-II expression—increased after late chronological aging in the Acyc 12m group, whereas the mid-aging group (9 months) trended to show an increase in the reactivity marker (Figures 3F and 3I). These data suggest that microglial mitochondrial oxidative stress and phagocytic capacity are inversely associated during endocrine aging. Dynamic shifts in microglial cells contributing to oxidative stress and phagocytic activity in the brain indicate a shift in the neural milieu during endocrine aging and the activation of an acute microglial response.

Astrocytic and Microglial Mitochondrial Function Are Differentially Expressed across Chronological and Endocrinological Aging

Evidence thus far suggested that chronological and endocrinological aging impact microglial reactivity, free radical generation, and phagocytic capacity. We hypothesized that microglial and astrocytic metabolic status would reflect the transitions in the neuroimmune phenotype. To test this hypothesis, metabolic

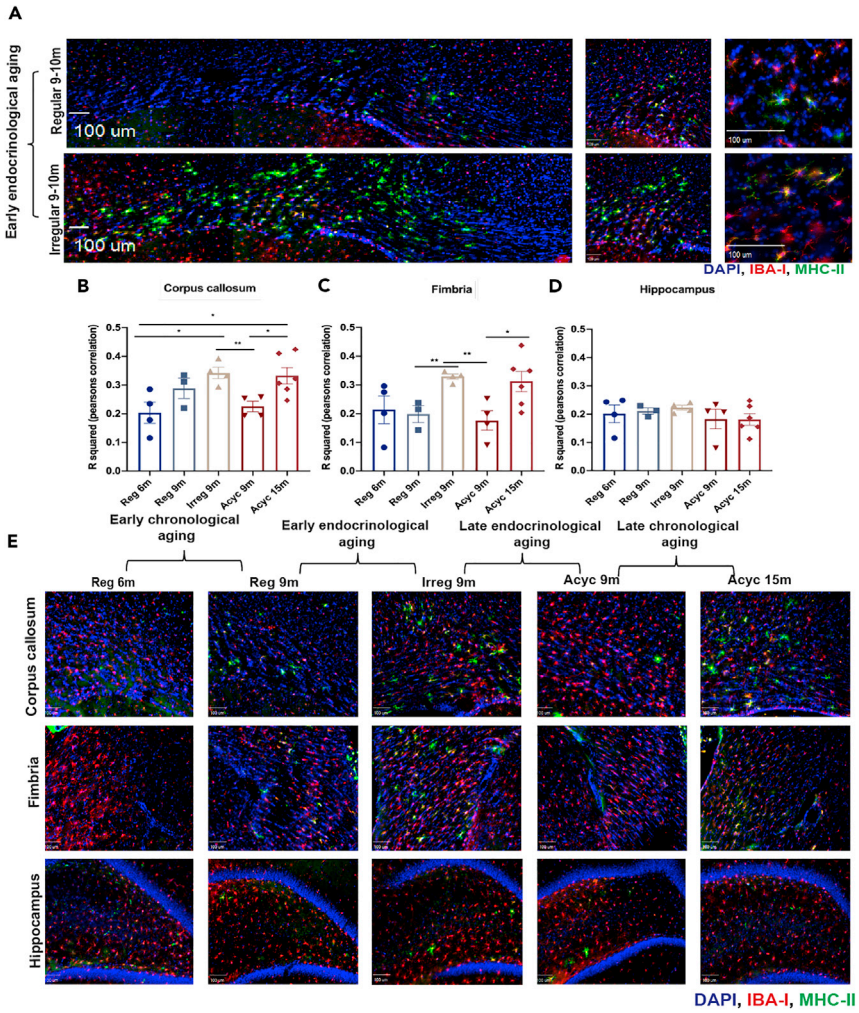

Figure 2. Spatial Mapping of Microglial Reactivity in the Female Aging Rat Brain

(A–D) Several regions in the brain were mapped for microglial reactivity by staining for microglial marker IBA-I (red) and reactivity marker, MHC-II (green), and DAPI (blue). (A) Representative images demonstrating the colocalization of MHC-II with IBA-I and the spatial distribution and differences in extent of MHC-II upregulation in the corpus callosum between Reg 9m and Irreg9m groups (scale bars, 100 μm). Quantification of the colocalization signals between IBA-I and MHC-II using Pearson's correlation in the (B) corpus callosum, (C) fimbria, and (D) hippocampus across five biological groups. (E) Representative images demonstrating the spatial mapping of IBA-I and MHC-II in the corpus callosum, fimbria, and hippocampus across the 5 biological groups (scale bars, 100 μm). Data are represented as mean ± SEM. *$p \leq 0.05$, **$p \leq 0.01$; calculated using unpaired-student t test.

status of glial cells, pooled from cortex, hippocampus, and white matter regions was investigated by measuring microglial and astrocytic mitochondrial respiratory capacity in primary cultures of microglia and astrocytes derived from 6-month-old and 12-month-old animals.

Microglial maximal respiration and ATP production, although not significantly affected, trended higher in younger 6-month-old animals (Figures 4A and 4B). However, microglia from the 12-month-old female brain exhibited significantly higher non-mitochondrial oxygen consumption.

Astrocytes derived from 12-month-old female brain exhibited a distinct spare respiratory phenotype. Consistent with increased β-oxidation (Jiang and Cadenas, 2014), astrocytic maximal respiration and spare respiratory capacity was significantly increased (Figures 4C and 4D), whereas basal respiration, proton leak, and ATP production were not impacted.

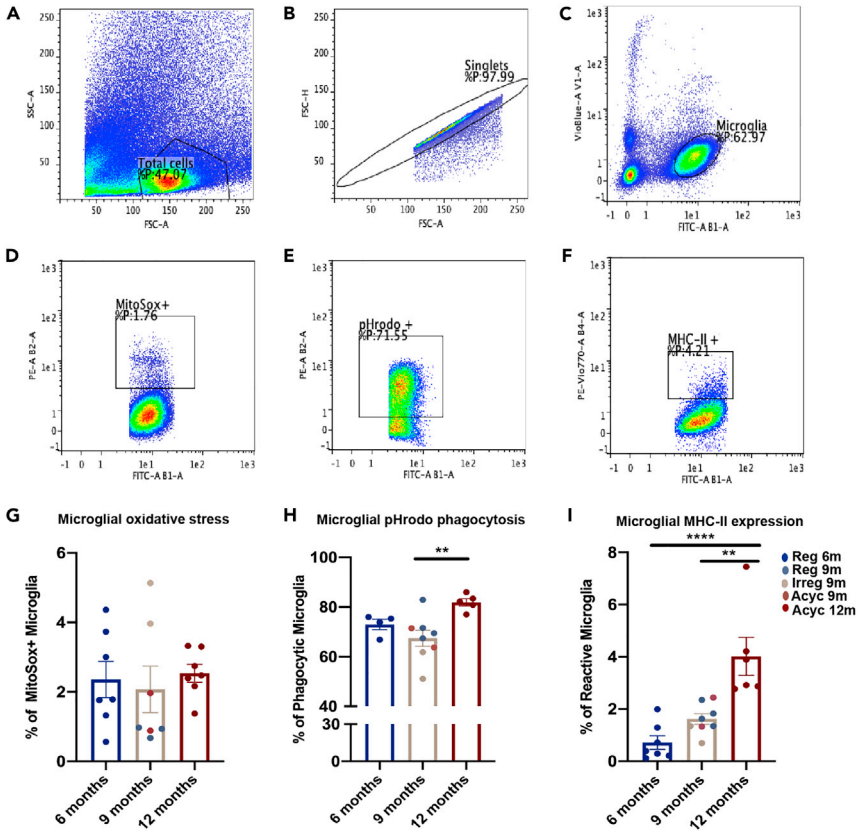

Figure 3. Microglial Oxidative Stress, Function, and Reactivity Across Chronological and Endocrinological Aging

(A–F) Figures A–F are representative figures of the gating strategy utilized for the assessment. Microglia were selected from the single cell suspension by first gating for (A) total cells from the suspension, then (B) singlets, and (C) then gating for microglia using CD11b (FITC) high and CD45 (Vio-Blue) intermediate as a gating strategy. Microglial cells expressing CD11b (FITC) were used for gating for (D) mitochondrial oxidative stress (PE) (E) output of phagocytic capacity (PE) and (F) MHC-II expression (PE-Vio770).

(G–I) (G) Quantification of mitochondrial oxidative stress. (H) Quantification of phagocytic capacity. (I) Quantification of MHC-II expression. Data are represented as mean ± SEM. *p ≤ 0.05, **p ≤ 0.01, ***p ≤ 0.001, ****p ≤ 0.0001 calculated using one-way ANOVA.

These data suggest that microglia and astrocytes react differently to chronological aging. The mechanisms to compensate for increased energy demand due to increased inflammation had a cell-specific difference, addressing their broader role in initiating, amplifying, and regulating inflammatory signals.

Estradiol Modulates Neuroinflammation in the Aging Female Brain

To investigate if the hippocampal transcriptome neuroinflammatory profile observed during chronological and endocrinological aging was due to depletion in steroidal hormones, 6-month-old female rats were ovariectomized (OVX). To determine if estradiol would mitigate neuroinflammation and the reactive phenotype of glial cells, two interventions were introduced: an estradiol prevention versus an estradiol treatment paradigm. The prevention paradigm was initiated 24 h post-OVX and was administered over a period of 5 weeks, whereas estradiol treatment paradigm was initiated 2 weeks following OVX and was 3 weeks in duration. Experimental paradigm for both groups equaled 5 weeks.

Bulk RNA-Seq of the hippocampus revealed that ovariectomy induced an upregulation of genes involved in type I and type II interferon response (*B2m*, *Irf7*, *Ifngr1*, *Fcer1g*) (Figure 5A and Table S2), a gene expression pattern previously observed during endocrine aging (Irreg 9m). Ovariectomy also induced an upregulation of genes involved in the complement system and *Trem2* (Figure 5B and Table S2), which was previously observed in the chronological aging phases preceding the perimenopause (Figure 1).

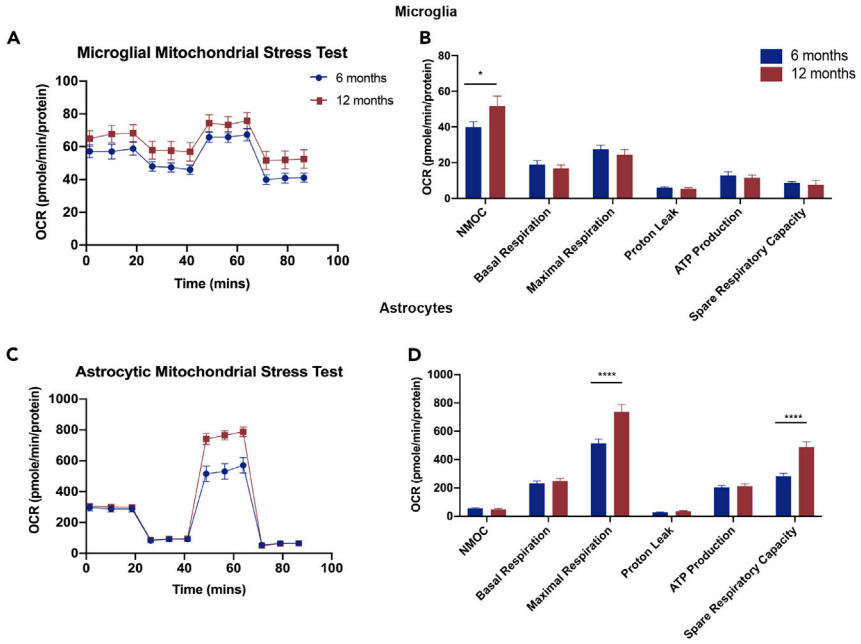

Figure 4. Mitochondrial Respiratory Capacity in Glial Cells across Age

Seahorse XFe24 analyzer was used to conduct metabolic flux assays on astrocytes and microglia derived from 6-month to 12-month-old female brains.

(A–D) (A) Microglia: oxygen consumption rate (OCR) normalized to protein in microglia. (B) Microglial mitochondrial function parameters. (C) Astrocytes: oxygen consumption rate (OCR) normalized to protein in astrocytes. (D) Astrocytic mitochondrial function parameters. NMOC - Non-Mitochondrial Oxygen Consumption. Data are represented as mean ± SEM. *p ≤ 0.05, ****p ≤ 0.0001; calculated by using two-way ANOVA and Sidak multiple test correction.

Estradiol prevention paradigm induced robust suppression of genes involved in the interferon response and the complement system (Figures 5A and 5B). In contrast, the estradiol treatment paradigm partially mitigated the effect of ovariectomy with a decrease in *B2m*, *Casp4*, *Irf7*, and *Fcer1g* expression, indicating a decrease in interferon response. However, multiple genes involved in the interferon response (*Ifit3*, *Ifngr1*, MHC: *Rt1-A2*), *C1s* and *Trem2*, were not suppressed and remained unaffected in the estradiol treatment paradigm (Figures 5A and 5B).

These data suggest that estradiol depletion by ovariectomy induced upregulation of type I and type II interferon responses, which was prevented by introducing estradiol 24 h after ovariectomy. In contrast, delay of estradiol treatment induced a partial, but not complete, suppression of type I and II interferon responses.

Human Validation of Neuroinflammatory Gene Expression in Hippocampus across Aging in Women and Evaluation of Sex Differences

To determine the translational validity of the inflammatory gene expression profile from the chronological and endocrinological midlife aging in perimenopausal animal model, we conducted a proof-of-concept analysis of hippocampal gene expression analysis using a dataset listed uner Gene Expression Omnibus (GEO): GSE11882 (Berchtold et al., 2008) and GEO2R tool of gene expression microarray data collected in human samples. Three age groups, 20–34 years, 35–59 years, and 60–75 years (accession numbers are listed in Tables S3 and S4), designed to capture pre-menopausal/young-adult, peri-to-menopausal/mid-life adult, and post-menopausal/late-life adult, respectively were investigated for differentially expressed genes. Gene expression profiles of age-matched men were analyzed in parallel. In women, multiple immune system related genes were within the top significantly different 250 genes across the age groups. Consistent with our preclinical findings, expression of MHC-I and -II, increased with age (Figure 6). MHC-II expression especially, *HLA-DMA*, *HLA-DMB*, *HLA-DQA1*, *HLA-DRB1*, *HLA-DRB6*, was increased during mid-life (35–59 years) relative to 20–34 years—young-adult group. Late-life phase in women was

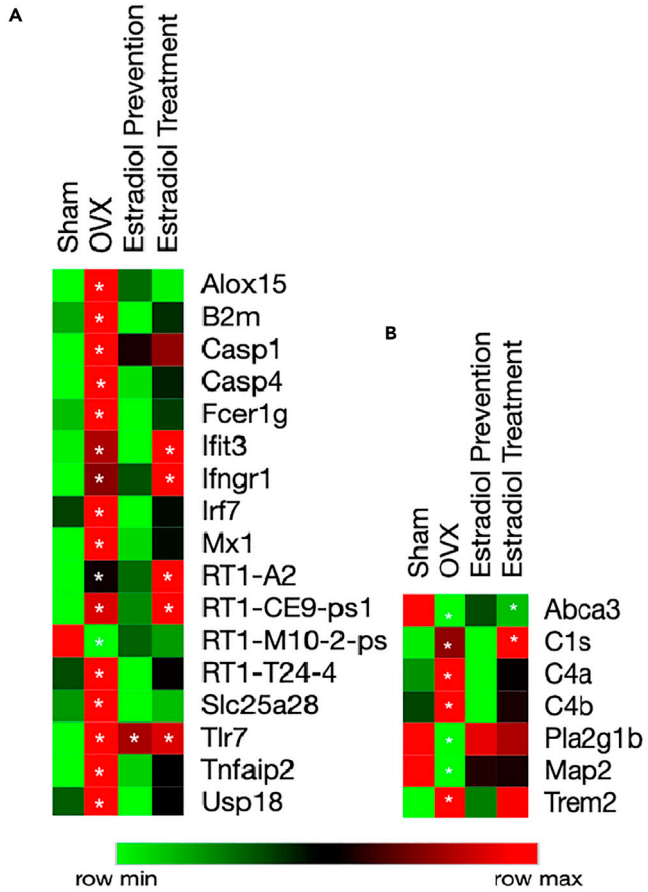

Figure 5. Estradiol Modulates Neuroinflammation in the Aging Female Brain

(A) Heatmap analysis of interferon response genes in the hippocampus, showing ovariectomy causes an upregulation. (B) Heatmap analysis of genes contributing to inflammation, myelin metabolism, and neuronal markers, indicating ovariectomy impacts the systems. All genes shown in heatmap are $p < 0.05$ for OVX versus SHAM. *$p < 0.05$ for differential gene expression analysis with respect to Sham;calculated using student t-test. Detailed p values<0.05 are listed in Table S2.

associated with an increased expression of MHC-II genes—*HLA-DMA*, *HLA-DQB1*, *HLA-DRA*, *HLA-DRB6*—by 2- to 10-fold (Figure 6A) relative to the early aging group (20–34 years).

In age-matched men, a similar pattern of MHC-II gene expression occurred with increasing age. However, the magnitude of increase, 1- to 3-fold, was lower than the 2- to 10-fold increase in age-matched women. The number of significantly affected genes in men was also less than women. Unlike women, a significant increase in men in MHC-II was only evident by *HLA-DRB1* gene expression during late life between 60 and 75 years (Figure 6B).

Microglial and neuronal communication genes that changed in the perimenopausal animal model were affected during aging in females and males. Microglial phagocytic receptor *TREM2* and *TYROBP* increased with aging in both females and males, although to a greater extent in females (Figures 6C and 6D). Interestingly, the microglial marker *CX3CR1*, which is involved in microglial checkpoint inhibition and homeostatic control (Deczkowska et al., 2018; Lee et al., 2010), was significantly upregulated during mid-life (35–59) years only in females (Figure 6C). The ligand for *CX3CR1* expressed on neurons, *CX3CL1*, showed a similar pattern in expression as *CX3CR1* in both females and males (Figures 6C and 6D). The *CD200* neuronal communication marker expression was not significantly affected but followed a similar pattern of expression in female and male aging, where it increased during mid-aging and decreased during late-aging phases (Figures 6C and 6D).

These data indicate that the rodent model recapitulates multiple aspects of neuroimmune aging in women. The magnitude of MHC-II upregulation was much higher in females than males. Gene expression of

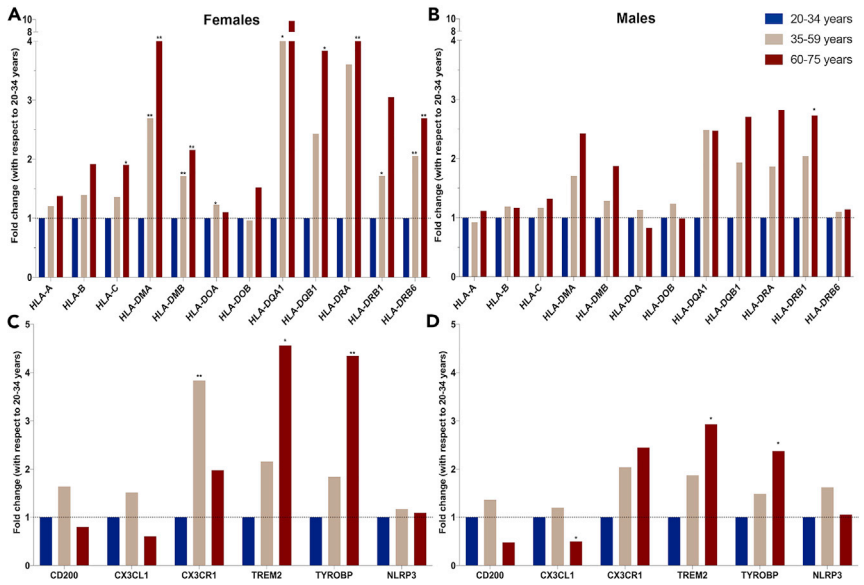

Figure 6. Translational Validation of Neuroinflammatory Gene Expression Profile

(A–D) Hippocampal gene expression analysis was conducted on Gene Expression Omnibus (GEO):GSE11882 on stratified age groups in females and males. Fold changes computed by GEO2R tool are plotted. MHC-II expression stratified by age in (A) females and (B) males. Markers for microglial and neuron communication stratified by age in (C) females and (D) males. Plotted as fold change with respect to 20–34 years as control. *p $\leq$ 0.05, **p $\leq$ 0.01, ***p $\leq$ 0.001 calculated by GEO2R tool.

microglial markers and checkpoint genes was also consistent with preclinical findings. These data highlight that aging with respect to inflammation in the hippocampus is dynamic and greater in magnitude in females relative to males.

DISCUSSION

Using an animal model that closely resembles the human perimenopausal transition, we investigated unique contributions of chronological and endocrinological female aging to neuroimmune profiles in brain. This study is the first to characterize chronological and endocrinological effect of aging of the neuroimmune system in brain with specific emphasis on brain regions most impacted in AD.

Hippocampal transcriptomic profiling indicated that inflammation was not a linear continuum in female aging brain. Each aging window was typified by a distinctive neuroimmune program. Chronological aging preceding the endocrinological perimenopause was marked by distinct upregulation in a subset of genes associated with disease-associated microglial phenotype (*Apoe*, *Trem2*, *Tyrobp*, *B2m*) and microglial reactivity markers such as *Aif1*, *C3*, and *Cd68*. This early chronological aging window was associated with a sustained downregulation of *Cd200*, a neuronal marker that participates in checkpoint inhibition of microglial phagocytic responses (Deczkowska et al., 2018). Subsequent to early phase chronological aging, the endocrinological aging phase was typified by upregulation of type I and II interferon response genes (*B2m*, *Irf1*, *Irf4*, *Ifnar2*, adhesion molecule *Vcam-1*) and downregulation of TGF-β signaling, *Apoe*, *Trem2*, *Tyrobp*, and microglial reactivity markers. The onset of reproductive senescence induced downregulation of type I and II interferon response genes and MHC-II genes. Late-phase chronological aging of post-menopause was specifically marked by upregulation of MHC-II genes, TNF signaling, phospholipases, lysosomal marker *Cd68*, and T cell marker *Cd4*. The gene expression profile is consistent with the onset of adaptive immune responses and white matter catabolism.

Recent characterization of models of familial AD and neurodegeneration (5xFAD, CK-p25) revealed a distinct phenotype of microglia, which is disease state specific and involves the participation of type I and type II interferon response genes, MHC, *Apoe*, *Trem2*, *Tyrobp*, and TGF-β signaling (Keren-Shaul et al., 2017; Mathys et al., 2017). Herein, we reported that female aging and specifically the perimenopausal transition is associated with a molecular signature of microglia associated with neurodegeneration. Of

note, the upregulation of type I and type II interferon response genes during the perimenopausal phase followed by the subsequent upregulation of MHC-II genes in the post-menopausal aged animals matches the "late response microglia" in the CK-p25 model (Mathys et al., 2017). Consistent with the expression of "late stage microglia" in neurodegeneration, the menopausal transition indicates that neurodegenerative programs can be activated early during midlife aging, possibly indicating the onset of a prodromal state.

Mapping of microglial reactivity revealed distinct localization of microglia to multiple white matter tracts that was coincident with early endocrine aging. Increased expression of MHC-II was evident in the corpus callosum, cingulum, and fimbria. Reduction in microglial phagocytosis was associated with age-related increase in myelin debris (Safaiyan et al., 2016), suggesting that the increase in MHC-II expression in white matter tracts observed during early endocrine aging is likely due to an increase in myelin debris. Microglial isolation from gray and white matter areas and subsequent functional profiling documented decline in phagocytosis during perimenopause. This microglial phenotype coupled with microglial mitochondrial respiratory phenotype and white matter track localization parallels earlier analyses of white matter catabolism for ketone body generation in brain during endocrine aging (Klosinski et al., 2015).

Microglial and astrocytic mitochondrial function paralleled immune phenotypic shifts during chronological and endocrinological aging. Microglia initiate the inflammatory response, whereas astrocytes amplify the inflammatory signals while meeting neuronal metabolic demands (Yin et al., 2016). Herein, we show that astrocytic maximal respiration and spare respiratory capacity and microglial non-mitochondrial oxygen consumption increased with age. The disparity between the cellular mitochondrial response to aging can be addressed by their broader function in the brain. Microglia respond to aging by increasing non-mitochondrial oxygen consumption, which possibly indicates increased anaerobic glycolysis and free radical production (Ghosh et al., 2018). Consistent with peripheral immune cells, microglia also react to inflammatory challenges by increasing anaerobic glycolysis and reduced mitochondrial respiration (Holland et al., 2018). In contrast, astrocytes increased spare respiratory capacity and maximal respiration, which is consistent with increased β-oxidation or response to energy demand of increased inflammation or both (Jiang and Cadenas, 2014).

Decline in estrogen during mid-life endocrine aging in the female is associated with a decline in glucose metabolism and activation of increased reliance on lipid-derived ketone bodies that can be supplied by white matter (Klosinski et al., 2015). Those analyses demonstrated a phased trajectory of white matter degeneration, lipid metabolism, and ketone body generation during endocrine aging (Klosinski et al., 2015). Consistent with increased mitochondrial oxidative stress reported herein, Klosinski et al. observed an increase in hydrogen peroxide production during early endocrine aging that activated the arachidonic acid and phospholipase A2 signaling pathways to activate sphingomyelinase metabolism of sphingomyelin followed by a staged activation of ceramidase and thiolase to generate fatty acid lipids that ultimately results in ketone body generation (Klosinski et al., 2015). The increase in maximal respiration and spare respiratory capacity in astrocytes with age is consistent with increased age-related inflammation (Jiang and Cadenas, 2014) and increased β-oxidation to generate ketone bodies (Klosinski et al., 2015). These findings in translational rodent models are consistent with human brain imaging, indicating that endocrine aging in women of perimenopausal to postmenopausal age exhibit decline in white matter volume and a rise in β-amyloid plague deposition (Mosconi et al., 2017a, 2017b, 2018).

Estrogen is a master regulator controlling neuronal and glial bioenergetics, neurogenesis, microglial inflammation, and glucose metabolism (Rettberg et al., 2014). Evidence for regulation of the inflammatory phenotype by estradiol is evident in the hippocampal transcriptomic profiling of ovariectomized animals. Ovariectomizing animals prior to onset of endocrine aging induced gene expression patterns that were a combination of chronological and endocrinological aging. Ovariectomy induced a transcriptomic profile indicative of accelerated aging in which early chronological and endocrinological aging (perimenopause) and late endocrinological aging are compressed into a single immune state (upregulation of *C4b*, *Trem2*, *Clec7a*, type I and II interferon response, MHC-I genes). Interestingly, ovariectomy did not cause significant changes in MHC-II expression, indicating that upregulation of MHC-II expression in aged reproductive senescent animals was in part caused by aging. Although ovariectomy mechanistically validates that estradiol regulates the neuroinflammatory phenotype, it also indicates that eliminating natural endocrine aging by ovariectomy causes an overt inflammatory reaction that combines inflammatory programs of chronological and endocrinological aging. The translational implication of accelerated immune reactivity is consistent

with earlier clinical studies, indicating increased risk of Alzheimer in women oophorectomized prior to natural menopause (Rocca et al., 2008, 2014). The estradiol prevention treatment paradigm prevented ovariectomy-induced immune profile, whereas the estradiol treatment paradigm failed to restore the pre-ovariectomy immune profile. Mitigation of inflammation and especially interferon response genes by an estradiol prevention treatment paradigm could be effective for disease-state-specific targeting of inflammation in prodromal states of AD. Epidemiological data provide support for reduced risk of AD in women treated with estrogen or hormone therapy for menopausal symptoms (Brinton, 2008), whereas treatment of postmenopausal women in the absence of symptoms has no benefit and depending on the hormone formulation can increase risk in women aged 65 years or older (Brinton, 2008).

Microglial activation of T cells mediated by type I and type II interferon is also at the core of pathophysiology of multiple sclerosis, an autoimmune disorder more prevalent in women than men (Schetters et al., 2018) and a worsening in the clinical trajectory following menopause.

Clinical gene expression analysis of differentially expressed genes in females during aging (20–34 years: early-life, 35–59 years: mid-life; and 60–75 years: late-life and reproductively senescent) was consistent with our rodent brain analyses. As endocrine aging status of the clinical samples was unavailable, stratification of groups was based on average age of perimenopausal to menopausal transition. Incremental upregulation of MHC-II and interferon response genes with age in females is indicative of immune activation in the brain after menopause. These findings suggest that the interferon and MHC signaling are likely linked to estrogen decline in the female brain (Wang et al., 2020).

Outcomes of analyses reported herein demonstrate dynamic shifts in the neuroinflammatory phenotype across chronological and endocrine aging in the female brain. Coincident with dysregulation of glucose metabolism during the perimenopausal transition in female brain (Ding et al., 2013a, 2013b; Klosinski et al., 2015; Wang et al., 2020; Yin et al., 2015) is the upregulation of interferon response and MHC-II expression in the hippocampus and white matter tracts. The inflammatory phenotype and upregulation of interferon response and MHC-II genes observed in the perimenopausal model was validated in ovariectomized animal models and human transcriptome data. Glial redox status, phagocytic capacity, and respiratory capacity also paralleled aging transitions. These findings highlight that the perimenopausal transition causes a significant shift in neuroinflammation, affecting glial function and metabolism.

Herein we report the emergence of neuroimmune responses in brain that emerge during midlife chronological and endocrinological aging transitions in the female brain. The profile of neuroimmune responses were dynamic, localized to white matter and unique to the stage of aging. The data supporting this complex biology are consistent across investigational methods, relevant to earlier fundamental and clinical science reports and have translational validity to the human. From a therapeutic perspective, these findings provide a foundation upon which to create a precision therapeutic strategy to prevent, delay, or treat neuroinflammation as an initiating and accelerating driver of Alzheimer risk in women.

Limitations of the Study

Although we provide evidence of upregulation of MHC-II in menopausal and post-menopausal aged women in a human micro-array dataset, these findings are not controlled for confounding variables. These analyses were conducted as a proof-of-concept evaluation and require replication in larger datasets. Furthermore, causal relationships between the upregulation of interferon response with metabolic dysfunction in brain requires further investigation. Notably, the role of microglial and astrocytic crosstalk in female brain aging needs to be further characterized. Interventional studies of MHC-II and interferon signaling therapeutics to investigate impact on white matter integrity, inflammation, and cognition could validate the role of interferon signaling in the aging female brain. Aging transitions that lead to the development of autoimmune profile such as multiple sclerosis and neurodegenerative diseases such as Alzheimer's require further exploration.

Resource Availability

Lead Contact

Further information and requests for resources and reagents should be directed to and will be fulfilled by the Lead Contact, Roberta Diaz Brinton (rbrinton@arizona.edu)

Data Availability

The accession number for the hippocampal RNA-Seq data from the perimenopausal animal model analyzed in this paper is GEO: GSE161142. The accession number for the hippocampal RNA-Seq datas from the ovariectomy, estradiol treatment, and prevention experiment analyzed in this paper is GEO: GSE161233.

METHODS

All methods can be found in the accompanying Transparent Methods supplemental file.

SUPPLEMENTAL INFORMATION

Supplemental Information can be found online at https://doi.org/10.1016/j.isci.2020.101829.

ACKNOWLEDGMENTS

This work was supported by NIH: National Institute on Aging, United States grants P01-AG026572 to R.D.B.; Project 1 to R.D.B. and Analytic Core to F.Y., R37AG053589 and, 1R01AG057931 to R.D.B.

AUTHOR CONTRIBUTIONS

Conceptualization, A.M. and R.D.B; Methodology, A.M., Y.S, Y.W., and E.B.; Formal analysis, A.M, Y.S., and F.Y.; Investigation, A.M.; Writing—Original Draft, A.M. and R.D.B.; Writing—Review and Editing, A.M. and R.D.B; Funding acquisition, R.D.B. and F.Y.

DECLARATION OF INTEREST

The authors declare no competing financial interest.

Received: June 16, 2020
Revised: October 13, 2020
Accepted: November 16, 2020
Published: December 18, 2020

REFERENCES

Akiyama, H., Barger, S., Barnum, S., Bradt, B., Bauer, J., Cole, G.M., Cooper, N.R., Eikelenboom, P., Emmerling, M., Fiebich, B.L., et al. (2000). Inflammation and Alzheimer's disease. Neurobiol. Aging *21*, 383–421.

Association, A.s. (2018). 2018 Alzheimer's disease facts and figures. Alzheimer's Demen. *14*, 367–429.

Bacon, E.R., Mishra, A., Wang, Y., Desai, M.K., Yin, F., and Brinton, R.D. (2019). Neuroendocrine aging precedes perimenopause and is regulated by DNA methylation. Neurobiology of aging *74*, 213–224.

Berchtold, N.C., Cribbs, D.H., Coleman, P.D., Rogers, J., Head, E., Kim, R., Beach, T., Miller, C., Troncoso, J., Trojanowski, J.Q., et al. (2008). Gene expression changes in the course of normal brain aging are sexually dimorphic. Proc. Natl. Acad. Sci. *105*, 15605.

Brinton, R.D. (2008). The healthy cell bias of estrogen action: mitochondrial bioenergetics and neurological implications. Trends Neurosciences *31*, 529–537.

Brinton, R.D., Yao, J., Yin, F., Mack, W.J., and Cadenas, E. (2015). Perimenopause as a neurological transition state. Nat. Rev. Endocrinol. *11*, 393–405.

Chung, H.Y., Kim, D.H., Lee, E.K., Chung, K.W., Chung, S., Lee, B., Seo, A.Y., Chung, J.H., Jung, Y.S., Im, E., et al. (2019). Redefining chronic inflammation in aging and age-related diseases: proposal of the senoinflammation concept. Aging Dis. *10*, 367–382.

Da Silva, J.A. (1995). Sex hormones, glucocorticoids and autoimmunity: facts and hypotheses. Ann. Rheum. Dis. *54*, 6–16.

Deczkowska, A., Amit, I., and Schwartz, M. (2018). Microglial immune checkpoint mechanisms. Nat. Neurosci. *21*, 779–786.

Ding, F., Yao, J., Rettberg, J.R., Chen, S., and Brinton, R.D. (2013a). Early decline in glucose transport and metabolism precedes shift to ketogenic system in female aging and Alzheimer's mouse brain: implication for bioenergetic intervention. PLoS One *8*, e79977.

Ding, F., Yao, J., Zhao, L., Mao, Z., Chen, S., and Brinton, R.D. (2013b). Ovariectomy induces a shift in fuel availability and metabolism in the hippocampus of the female transgenic model of familial Alzheimer's. PLoS One *8*, e59825.

Eikelenboom, P., Zhan, S.-S., van Gool, W.A., and Allsop, D. (1994). Inflammatory mechanisms in Alzheimer's disease. Trends Pharmacol. Sci. *15*, 447–450.

Ghosh, S., Castillo, E., Frias, E.S., and Swanson, R.A. (2018). Bioenergetic regulation of microglia. Glia *66*, 1200–1212.

Griffin, W.S.T. (2006). Inflammation and neurodegenerative diseases. Am. J. Clin. Nutr. *83*, 470S–474S.

Gubbels Bupp, M.R., Potluri, T., Fink, A.L., and Klein, S.L. (2018). The confluence of sex hormones and aging on immunity. Front. Immunol. *9*, 1269.

Heneka, M.T., Carson, M.J., El Khoury, J., Landreth, G.E., Brosseron, F., Feinstein, D.L., Jacobs, A.H., Wyss-Coray, T., Vitorica, J., Ransohoff, R.M., et al. (2015). Neuroinflammation in Alzheimer's disease. Lancet Neurol. *14*, 388–405.

Holland, R., McIntosh, A.L., Finucane, O.M., Mela, V., Rubio-Araiz, A., Timmons, G., McCarthy, S.A., Gun'ko, Y.K., and Lynch, M.A. (2018). Inflammatory microglia are glycolytic and iron retentive and typify the microglia in APP/PS1 mice. Brain Behav. Immun. *68*, 183–196.

Itagaki, S., McGeer, P.L., Akiyama, H., Zhu, S., and Selkoe, D. (1989). Relationship of microglia and astrocytes to amyloid deposits of Alzheimer disease. J. Neuroimmunol. *24*, 173–182.

Jiang, T., and Cadenas, E. (2014). Astrocytic metabolic and inflammatory changes as a function of age. Aging cell *13*, 1059–1067.

Keren-Shaul, H., Spinrad, A., Weiner, A., Matcovitch-Natan, O., Dvir-Szternfeld, R., Ulland, T.K., David, E., Baruch, K., Lara-Astaiso, D., Toth, B., et al. (2017). A unique microglia type Associated with restricting development of Alzheimer's disease. Cell *169*, 1276–1290.e1217.

Klein, S.L., and Flanagan, K.L. (2016). Sex differences in immune responses. Nat. Rev. Immunol. *16*, 626.

Klosinski, L.P., Yao, J., Yin, F., Fonteh, A.N., Harrington, M.G., Christensen, T.A., Trushina, E., and Brinton, R.D. (2015). White matter lipids as a ketogenic fuel supply in aging female brain: implications for alzheimer's disease. EBioMedicine *2*, 1888–1904.

Lee, S., Varvel, N.H., Konerth, M.E., Xu, G., Cardona, A.E., Ransohoff, R.M., and Lamb, B.T. (2010). CX3CR1 deficiency alters microglial activation and reduces beta-amyloid deposition in two Alzheimer's disease mouse models. Am. J. Pathol. *177*, 2549–2562.

Lynch, M. (2010). Age-related neuroinflammatory changes negatively impact on neuronal function. Front. Aging Neurosci. *1*, 6.

Márquez, E.J., Chung, C.-h., Marches, R., Rossi, R.J., Nehar-Belaid, D., Eroglu, A., Mellert, D.J., Kuchel, G.A., Banchereau, J., and Ucar, D. (2020). Sexual-dimorphism in human immune system aging. Nat. Commun. *11*, 751.

Mathys, H., Adaikkan, C., Gao, F., Young, J.Z., Manet, E., Hemberg, M., De Jager, P.L., Ransohoff, R.M., Regev, A., and Tsai, L.-H. (2017). Temporal tracking of microglia activation in neurodegeneration at single-cell resolution. Cell Rep. *21*, 366–380.

Mattiace, L.A., Davies, P., Yen, S.H., and Dickson, D.W. (1990). Microglia in cerebellar plaques in Alzheimer's disease. Acta Neuropathologica *80*, 493–498.

McCruden, A.B., and Stimson, W.H. (1991). Sex hormones and immune function, R. Ader, D.L. Felten Psychoneuroimmunology and N. Cohen, eds. (Academic Press), pp. 475–493.

McGeer, P.L., Akiyama, H., Itagaki, S., and McGeer, E.G. (1989). Immune system response in alzheimer's disease. Can. J. Neurol. Sci. *16*, 516–527.

McGeer, P.L., Itagaki, S., Tago, H., and McGeer, E.G. (1987). Reactive microglia in patients with senile dementia of the Alzheimer type are positive for the histocompatibility glycoprotein HLA-DR. Neurosci. Lett. *79*, 195–200.

Mishra, A., and Brinton, R.D. (2018). Inflammation: bridging age, menopause and APOEε4 genotype to Alzheimer's disease. Front. Aging Neurosci. *10*, 312.

Mosconi, L., Berti, V., Quinn, C., McHugh, P., Petrongolo, G., Osorio, R.S., Connaughty, C., Pupi, A., Vallabhajosula, S., Isaacson, R.S., et al. (2017a). Perimenopause and emergence of an Alzheimer's bioenergetic phenotype in brain and periphery. PLoS One *12*, e0185926.

Mosconi, L., Berti, V., Quinn, C., McHugh, P., Petrongolo, G., Varsavsky, I., Osorio, R.S., Pupi, A., Vallabhajosula, S., Isaacson, R.S., et al. (2017b). Sex differences in Alzheimer risk: brain imaging of endocrine vs chronologic aging. Neurology *89*, 1382–1390.

Mosconi, L., Rahman, A., Diaz, I., Wu, X., Scheyer, O., Hristov, H.W., Vallabhajosula, S., Isaacson, R.S., de Leon, M.J., and Brinton, R.D. (2018). Increased Alzheimer's risk during the menopause transition: a 3-year longitudinal brain imaging study. PLoS One *13*, e0207885.

Nebel, R.A., Aggarwal, N.T., Barnes, L.L., Gallagher, A., Goldstein, J.M., Kantarci, K., Mallampalli, M.P., Mormino, E.C., Scott, L., Yu, W.H., et al. (2018). Understanding the impact of sex and gender in Alzheimer's disease: a call to action. Alzheimer's Demen. *14*, 1171–1183.

Niu, H., Álvarez-Álvarez, I., Guillén-Grima, F., and Aguinaga-Ontoso, I. (2017). Prevalence and incidence of Alzheimer's disease in Europe: a meta-analysis. Neurología (English Edition) *32*, 523–532.

Rettberg, J.R., Yao, J., and Brinton, R.D. (2014). Estrogen: a master regulator of bioenergetic systems in the brain and body. Front. neuroendocrinology *35*, 8–30.

Rocca, W.A., Grossardt, B.R., and Maraganore, D.M. (2008). The long-term effects of oophorectomy on cognitive and motor aging are age dependent. Neuro-degenerative Dis. *5*, 257–260.

Rocca, W.A., Grossardt, B.R., and Shuster, L.T. (2014). Oophorectomy, estrogen, and dementia: a 2014 update. Mol. Cell. Endocrinol. *389*, 7–12.

Roved, J., Westerdahl, H., and Hasselquist, D. (2017). Sex differences in immune responses: hormonal effects, antagonistic selection, and evolutionary consequences. Horm. Behav. *88*, 95–105.

Ruggieri, A., Gagliardi, M.C., and Anticoli, S. (2018). Sex-dependent outcome of hepatitis B and C viruses infections: synergy of sex hormones and immune responses? Front. Immunol. *9*, 2302.

Safaiyan, S., Kannaiyan, N., Snaidero, N., Brioschi, S., Biber, K., Yona, S., Edinger, A.L., Jung, S., Rossner, M.J., and Simons, M. (2016). Age-related myelin degradation burdens the clearance function of microglia during aging. Nat. Neurosci. *19*, 995–998.

Sanada, F., Taniyama, Y., Muratsu, J., Otsu, R., Shimizu, H., Rakugi, H., and Morishita, R. (2018). Source of chronic inflammation in aging. Front. Cardiovasc. Med. *5*, 12.

Sárvári, M., Hrabovszky, E., Kalló, I., Solymosi, N., Likó, I., Berchtold, N., Cotman, C., and Liposits, Z. (2012). Menopause leads to elevated expression of macrophage-associated genes in the aging frontal cortex: rat and human studies identify strikingly similar changes. J. Neuroinflammation *9*, 264.

Sárvári, M., Kalló, I., Hrabovszky, E., Solymosi, N., and Liposits, Z. (2014). Ovariectomy and subsequent treatment with estrogen receptor agonists tune the innate immune system of the Hippocampus in middle-aged female rats. PLoS One *9*, e88540.

Schetters, S.T.T., Gomez-Nicola, D., Garcia-Vallejo, J.J., and Van Kooyk, Y. (2018). Neuroinflammation: microglia and T cells get ready to tango. Front. Immunol. *8*, 1905.

Simen, A.A., Bordner, K.A., Martin, M.P., Moy, L.A., and Barry, L.C. (2011). Cognitive dysfunction with aging and the role of inflammation. Ther. Adv. Chronic Dis. *2*, 175–195.

Sohrabji, F. (2007). Guarding the blood-brain barrier: a role for estrogen in the etiology of neurodegenerative disease. Gene Expr. *13*, 311–319.

Straub, R.H. (2007). The complex role of estrogens in inflammation. Endocr. Rev. *28*, 521–574.

Van Eldik, L.J., Carrillo, M.C., Cole, P.E., Feuerbach, D., Greenberg, B.D., Hendrix, J.A., Kennedy, M., Kozauer, N., Margolin, R.A., Molinuevo, J.L., et al. (2016). The roles of inflammation and immune mechanisms in Alzheimer's disease. Alzheimer's Dementia (N Y) *2*, 99–109.

Wang, Y., Mishra, A., and Brinton, R.D. (2020). Transitions in Metabolic and Immune Systems from Pre-menopause to Post-menopause: Implications for Age-Associated Neurodegenerative Diseases*9*, p. F1000Res.

Wang, Y., Shang, Y., Mishra, A., Bacon, E., Yin, F., and Brinton, R. (2020). Midlife Chronological and Endocrinological Transitions in Brain Metabolism: System Biology Basis for Increased Alzheimer's Risk in Female Brain. Scientific Reports *10*, 8528.

Yao, J., and Brinton, R.D. (2012). Estrogen regulation of mitochondrial bioenergetics: implications for prevention of Alzheimer's disease. Adv. Pharmacol. *64*, 327–371.

Yao, J., Irwin, R., Chen, S., Hamilton, R., Cadenas, E., and Brinton, R.D. (2012). Ovarian hormone loss induces bioenergetic deficits and mitochondrial beta-amyloid. Neurobiol. Aging *33*, 1507–1521.

Yin, F., Sancheti, H., Patil, I., and Cadenas, E. (2016). Energy metabolism and inflammation in brain aging and Alzheimer's disease. Free Radic. Biol. Med. *100*, 108–122.

Yin, F., Yao, J., Sancheti, H., Feng, T., Melcangi, R.C., Morgan, T.E., Finch, C.E., Pike, C.J., Mack, W.J., Cadenas, E., et al. (2015). The perimenopausal aging transition in the female rat brain: decline in bioenergetic systems and synaptic plasticity. Neurobiol. Aging *36*, 2282–2295.

Zhao, L., Mao, Z., Woody, S.K., and Brinton, R.D. (2016). Sex differences in metabolic aging of the brain: insights into female susceptibility to Alzheimer's disease. Neurobiol. Aging *42*, 69–79.

iScience, Volume *23*

Supplemental Information

Dynamic Neuroimmune Profile during Mid-life Aging in the Female Brain and Implications for Alzheimer Risk

Aarti Mishra, Yuan Shang, Yiwei Wang, Eliza R. Bacon, Fei Yin, and Roberta D. Brinton

Supplemental Information

Supplemental Tables

Table S1. P-value of significant fold changes in gene expression, related to Figure 1

	Gene name	Reg 9m		Irreg 9m		Acyc 9m		Acyc 15m	
		p-value	padj	p-value	padj	p-value	padj	p-value	padj
Microglial reactivity	Aif1	5.71E-04							
	Apoe	1.98E-02							
	Cd68	2.39E-03		4.70E-02		2.33E-03		2.51E-03	
	Cd200					3.02E-02			
	Fscn1			1.64E-04	4.96E-03				
	Itgb2	1.74E-03		4.66E-02		1.45E-04	8.52E-03	5.31E-03	
	Nlrp3			1.53E-03	1.94E-02	2.51E-03			
	Sirpa			9.96E-05	3.64E-03				
	Tgfa	6.33E-04		3.90E-03	3.58E-02			7.04E-03	
	Trem2	2.71E-04							
	Tyrobp	2.55E-04							
Complement	C1qa	6.25E-04				3.47E-02		3.68E-04	1.34E-02
	C1qb	1.67E-02							
	C3							3.65E-02	
	C3ar1								
	C4a	1.09E-06	1.48E-02	3.29E-02		6.76E-06	9.83E-04	5.41E-05	3.63E-03
	C4b	1.19E-02		3.32E-03	3.20E-02	5.35E-04		7.02E-03	
Lipid metabolism	Vegfa			3.67E-02					
	Siglec1			1.02E-03	1.51E-02	4.33E-02			
	Abca1	2.13E-03		9.92E-05	3.64E-03	1.29E-02		6.35E-03	
	Abca3			1.99E-02					
	Abca7	3.23E-02		1.17E-02		8.36E-04	2.51E-02	5.06E-04	1.66E-02
	Ide			3.64E-03	3.40E-02	1.61E-02			
	Nos3			3.54E-02					
	Pla2g10			3.07E-02					
	Pla2g15			3.77E-02					
	Pla2g4b			6.54E-03		7.74E-04	2.42E-02	1.02E-04	5.76E-03
	Sox10	5.56E-03							
	Sox13	2.39E-03		4.26E-02					
TGF-beta signaling	Acvrl1			4.84E-02		4.12E-03		4.61E-02	
	Bmpr1b			3.80E-04	8.21E-03	2.39E-03	4.70E-02	1.69E-02	
	Chrd			1.89E-02		4.17E-04	1.63E-02	5.72E-05	3.76E-03
	Mapk3			2.61E-03	2.75E-02				
	Nog			2.17E-03	2.41E-02	1.38E-02		9.78E-03	
	Ppp2r1a			2.46E-04	6.40E-03	3.45E-02			
	Ppp2r2b			1.00E-02					
	Rbx1			3.60E-04	7.97E-03	3.74E-08	3.29E-05	3.36E-08	2.13E-05
	Rps6kb1			2.16E-03	2.40E-02				
	Rps6kb2			2.51E-02		3.85E-02			
	Skp1			6.88E-03		6.58E-06	9.83E-04	7.03E-06	8.91E-04
	Smad5			6.02E-03	4.79E-02	2.90E-02			
	Sp1			3.12E-04	7.31E-03				
	Tgfb3			5.74E-03	4.65E-02				
	RT1-A1	4.72E-02							

MHC-I	RT1-CE10	2.10E-02						2.87E-03	
	RT1-CE4							1.36E-02	
	RT1-CE7							1.11E-02	
	RT1-T24-2	2.20E-02		2.81E-02					
	RT1-T24-3	3.05E-04		1.38E-03	1.82E-02	6.15E-03			
	RT1-M3-1			3.45E-02				9.31E-04	2.46E-02
MHC-II	RT1-Ba								
	RT1-Bb					3.44E-02		4.60E-02	
	RT1-Da								
	RT1-Db1								
	RT1-Db2							3.95E-02	
	RT1-DMb	1.99E-02							
TNF Signaling	Tnfaip3								
	Apaf1								
	Fos								
	Jun			2.02E-02		4.60E-02			
	Casp9								
	Casp2								
	Cycs			8.83E-03		5.67E-05		4.54E-02	
	Fadd								
	Map4k2			5.56E-04	1.03E-02	3.04E-06	5.77E-04	8.93E-06	1.05E-03
	Tank								
	Mapk8								
	Madd					3.40E-02		4.67E-02	
	LOC100912399			6.67E-04	1.15E-02				
	Map2k4								
	Map3k14								
	Casp8								
	Ripk1								
	Bid								
	Tnf								
	Tnfrsf1a								
	Tradd								
	Traf2								
Type I & II Interferon Response	B2m	5.23E-03		1.39E-02					
	Casp4			6.76E-03					
	Cfb	3.20E-03		1.85E-03					
	Cfh			9.69E-03					
	Ddx60			3.20E-02					
	Elf1			7.10E-03					
	Gbp2			2.95E-02					
	Gbp4			4.14E-02					
	Herc6	1.26E-02		3.03E-05	1.83E-03	5.22E-03			
	Ifi44	1.10E-02		3.95E-03	3.61E-02				
	Ifih1	1.02E-02		8.06E-04	1.30E-02	3.84E-02		8.57E-03	
	Ifit2			1.68E-02					

	Ifitm3	4.13E-05	4.57E-02	4.45E-06	5.11E-04	4.05E-03			
	Ifnar2			1.19E-02				1.29E-02	
	Il15ra			3.51E-02				3.33E-02	
	IL18BP			1.87E-02				3.62E-02	
	Irf1	5.97E-03		2.02E-02				5.44E-03	
	Irf2								
	Irf4	7.85E-03		4.16E-02					
	Irf7	6.95E-03							
	Itgb7								
	Lap3	8.19E-03		5.46E-03	4.51E-02			1.95E-05	1.94E-03
	Lpar6			1.38E-02					
	Ly6e			2.92E-04	7.01E-03	4.72E-02			
	Mov10			1.59E-02		4.99E-02			
	Mvp	1.72E-02		2.99E-02					
	Nampt			1.54E-02					
	Ncoa3			1.31E-02		3.25E-04			
	Nfkb1	1.56E-02				4.92E-02		3.20E-02	
	Nlrc5					3.58E-02		1.99E-02	
	Nmi	3.25E-02		3.79E-02					
	Nup93			3.62E-05		6.45E-04	2.13E-02	7.04E-04	2.06E-02
	Ogfr			5.52E-04	1.03E-02				
	P2ry14			1.22E-02					
	Parp9			1.29E-02		1.78E-02			
	Parp14	2.85E-02		2.35E-02					
	Plscr1	6.99E-03		1.98E-04	5.54E-03			2.66E-03	
	Ripk2			3.71E-03	3.46E-02				
	Rnf213	3.90E-03		4.24E-06		1.38E-04	8.31E-03	4.98E-04	1.64E-02
	Rsad2	2.22E-02		3.53E-03	3.34E-02	3.61E-02			
	Smad9			1.06E-02				1.50E-02	
	Sp110	9.03E-03		6.24E-03	4.92E-02	1.81E-02			
	Sspn	3.58E-02							
	St3gal5			1.96E-03				4.39E-02	
	Tnfaip6	9.81E-03							
	Trafd1			2.94E-03	2.99E-02			4.16E-03	
	Txnip			1.85E-02				2.03E-02	
	Uba7			9.39E-03		1.04E-02			
	Usp18	1.31E-02		2.97E-02					
	Vcam1	2.04E-02		9.03E-04	1.40E-02				
T cell	Cd3d								
	Cd3e								
	Cd3eap								
	Cd3g								
	Cd4							2.20E-04	9.65E-03
	Cd40								
	Cd40lg								
	Cd69								
	Socs1								
	Socs3								
	Mmp12								
	Cxcl9								
	Icam1							1.68E-02	

Table 1: P-value and adjusted-p value (padj) <0.05 of fold changes in hippocampal differential gene expression analysis of Reg 9m, Irreg 9m, Acyc 9m and Acyc 15m with respect to Reg 6m for heatmap analysis in Figure 1. Pathway analysis focused on in microglial reactivity, complement, lipid metabolism, Transforming Growth Factor -β (TGF-β) signaling, Major Histocompatibility Complex (MHC) class I and class II, Tumor Necrosis Factor (TNF) signaling, type I and type II interferon signaling and T cell markers and signaling with respect to Reg 6m

Table S2. P-value of significant fold changes in gene expression with respect to Sham, related to Figure 5

	Gene names	OVX	E2 Prevention	E2 Treatment
Type I & II Interferon Response	Alox15	8.17E-04		
	B2m	4.35E-02		
	Casp1	4.74E-02		
	Casp4	4.55E-02		
	Fcer1g	6.49E-03		
	Ifit3	4.36E-02		2.14E-02
	Ifngr1	2.98E-02		7.14E-03
	Irf7	9.94E-03		
	Mx1	3.31E-03		
	RT1-A2	2.30E-02		3.08E-03
	RT1-CE9-ps1	2.00E-02		1.70E-02
	RT1-M10-2-ps	2.06E-02		
	RT1-T24-4	1.87E-04		
	Slc25a28	2.64E-02		
	Tlr7	2.70E-03	2.60E-02	1.47E-02
	Tnfaip2	1.16E-02		
	Usp18	1.54E-02		
Inflammation, myelin metabolism and neuronal markers	Abca3	1.27E-02		4.69E-02
	C1s	2.66E-02		7.34E-03
	C4a	3.29E-03		
	C4b	1.66E-02		
	Pla2g1b	4.08E-02		
	Map2	1.67E-03		
	Trem2	2.39E-02		

Table 2. P-value<0.05 of fold changes in hippocampal differential gene expression analysis of genes involved in type I and II interferon response genes and genes participating in inflammation, myelin metabolism and neuronal markers, with respect to Sham (OVX: ovariectomized, E2: 17-β-estradiol).

Table S3. Age and hippocampal sample information used for female aging analysis from the GSE11882 dataset, related to Figure 6

Sex	Age group	Accession number	Age (years)
Female	20-34 years	GSM300219	34
		GSM300272	26
		GSM300298	30
	35-59 years	GSM300187	45
		GSM300231	37
		GSM300290	44
		GSM300294	48
		GSM300321	47
	60-75 years	GSM300190	74
		GSM300197	74
		GSM300223	74
		GSM300239	70
		GSM300243	64

Table S4. Age and hippocampal sample information used for male aging analysis from the GSE11882 dataset, related to Figure 6

Sex	Age group	Accession number	Age (years)
Male	20-34 years	GSM300276	20
		GSM300280	20
		GSM300301	20
		GSM300305	33
		GSM300309	22
	35-59 years	GSM300262	52
		GSM300313	42
		GSM300317	45
		GSM300174	45
	60-75 years	GSM300255	69
		GSM300286	69
		GSM300325	69
		GSM300333	75

Transparent Methods

Animals

All animal studies and procedures were conducted using the National Institutes of Health guidelines for procedures on laboratory animals. The procedures were approved by the University of Southern California and University of Arizona Institutional Care and Use Committee. Rats were housed in a facility with 12h light/dark cycle and food and water was supplied *ad libitum*.

Wild-type Sprague Dawley female rats of the ages of 5 months and 8 months were procured from Envigo laboratories (New Jersey, NJ, US). To establish the perimenopausal animal model used in this study (Yin et al., 2015), the animals were characterized for their reproductive cyclicity for a month using vaginal lavages conducted daily between 9 am and 11 am one week after they arrived(Bacon et al., 2019; Wang et al., 2020; Yin et al., 2015) . The vaginal lavages were fixed using 95% alcohol and stained using Giemsa stain for characterization of the cell types. A typical reproductive cycle of the female rat is defined by: Estrus (E) phase signified by large cornified cells, Metestrus (M) phase, which is marked by leukocytes, cornified cells and epithelial cells, Diestrus (D) phase marked by leukocytes and Proestrus (P) phase which can be identified by nucleated epithelial cells. During reproductively competent phases rats' cycle through the four phases (E, M, P and D) in 4-5 days, which is referred to as Regular cycling. Rats were enrolled into Regular 6-months (Reg 6m) or Regular 9-10-months (Reg 9m) group, if they had at least two consecutive regular cycles by the time of dissection. During the ages of 9-10 months, when the rats begin to transition to a reproductively incompetent phase the lengths of their cycles increase to 6-9 days, which is referred to as the reproductively irregular phase. Rats were enrolled into the Irregular 9-10-months (Irreg 9m) group if they had at least two consecutive irregular cycles. The onset of a reproductively senescent phase is established by 10-12-day long cycle usually composed of constant estrus, which is referred to as acyclic. Animals were enrolled into the Acyclic 9-10 months (Acyclic 9m) if they had been in constant estrus for 10 days or more. Animals that did not meet these criteria were aged further to 15-16 months. Animals were reproductively monitored for two weeks, and only animals that were constant estrus were used for the reproductively senescent group: Acyclic 15-16 months (Acyclic 15m). Animals were euthanized on the day of estrus to eliminate the confounding effects of the estrus cycle. The Reg 6m and Acyclic 15m groups were

used for studying the chronological aging phase preceding and succeeding the endocrinological transition phase. Comparison between Reg 6m and Reg 9m indicates early chronological aging group, whereas the comparison between Acyc 9m and Acyc 16m group indicates late-chronological aging phase. For understanding the effects of endocrinological aging without the confounding effects of aging the Reg 9m, Irreg 9m and Acyc 9m groups were used. Serum and cortical 17-β-estradiol ((8*R*,9*S*,13*S*,14*S*,17*S*)-13-methyl-6,7,8,9,11,12,14,15,16,17-decahydrocyclopenta[a]phenanthrene-3,17-diol) (E2) and progesterone ((8*S*,9*S*,10*R*,13*S*,14*S*,17*S*)-17-acetyl-10,13-dimethyl-1,2,6,7,8,9,11,12,14,15,16,17-dodecahydrocyclopenta[a]phenanthren-3-one) (P4) levels of the perimenopausal animal model were established in a previous study (Yin et al., 2015). The steroidal concentrations were measured using LC/MS-MS. Cortical E2 levels were highest in the Reg 6m group, significantly reduced on early chronological aging (Reg 9m) and became almost negligent in Acyc 9m and Acyc 16m groups. Serum E2 levels were highest in the Reg 9m group, and steadily declined on endocrinological and late-chronological aging and were lowest in the Acyc 16m group. Interestingly, serum E2 levels increased with early chronological aging. Cortical P4 levels were highest in the Reg 6m group, and declined with early chronological and endocrinological aging, Serum P4 levels were highest in the Irreg 9m group. A significant correlation between cortical and serum P4 levels was observed. For RNA-Seq N=6/group was used.

Ovariectomy, estradiol treatment and prevention:

A total of 40 rats were used for this experiment. Ovariectomy (OVX) or sham (SHAM) surgery was conducted on 6-month-old Sprague Dawley rats. A subset of ovariectomized rats were enrolled in the 17-β-estradiol ((8*R*,9*S*,13*S*,14*S*,17*S*)-13-methyl-6,7,8,9,11,12,14,15,16,17-decahydrocyclopenta[a]phenanthrene-3,17-diol) (E2) treatment (E2 Treatment) group. The treatment paradigm started 2 weeks after the surgery and included 3 weeks of estradiol treatment. Another subset of rats was enrolled in the estradiol prevention (E2 Prevention) group. The prevention paradigm started the day after the surgery and included 5 weeks of estradiol treatment. In the both the groups, 0.8 mg of E2 (10% E2 in cholesterol) was administered subcutaneously using silastic tubes (1.57mm inner diameter and 1cm length) and replaced every 30 days. Ovariectomized animals received cholesterol as vehicle treatment. Administration of treatment was based on a previously conducted study(Barron et al., 2015). Previous

pharmacokinetic studies have established that the serum estradiol concentration, with the dose of E2 administered, is around 40 pg/ml after 10 days of onset of treatment (Mannino et al., 2005). The serum estradiol levels match that of the proestrus stage of the reproductive cycle (Smith et al., 1975).Ovariectomized and sham animals were aged up to 5 weeks after the surgery. Animals used (N)= 5-7 animals/group.

Brain Dissection

Animals were anesthetized using intraperitoneal injection of ketamine (80 mg/kg) and xylazine (10 mg/kg). After a midline incision and lateral separation of the cranium, the whole brain was harvested from the skull. The brain was rapidly dissected on ice using a procedure previously described (Yin et al., 2015). Briefly, the meninges were peeled off following which the hypothalamus, cerebellum and brain stem were removed sequentially. The two hemispheres of the brain were separated. The cortex was peeled laterally, revealing the hippocampus which was rolled out. All the harvested brain regions were frozen on dry ice and stored at -80°C for further processing.

RNA extraction

The left hippocampus was cryopulverized and aliquoted for further processing. The tissue was homogenized in TRIzol™reagent (Invitrogen™, cat# 15596026) using 0.5 mL of regent per 20-30 mg of tissue. The tissue was homogenized using Bullet Blender™ and RNAase-free silicon beads for 3-5 mins at speed 6. The homogenized tissue was incubated with TRIzol™reagent for 5-7 minutes at RT. Chloroform was added to extract RNA, using a 1:5 ratio of chloroform: TRIzol™ reagent, and vigorously mixed. The mixture was centrifuged at 12,000 *g*, for 15 minutes at 4°C. The upper chloroform phase was separated and further purified using the PureLink® RNA mini kit (Invitrogen™, cat# 12185010) using the manufacturer's protocol. RNA was eluted using UltraPure™ water (Invitrogen™, cat# 10977015). RNA concentration and ratios to estimate RNA integrity, was measured on NanoDrop™ One (Thermo Scientific™,cat# ND-ONE-W).

RNA Sequencing (RNA-Seq)

For conducting unbiased discovery-based assessment of differentially expressed genes during female aging, RNA-Seq was conducted at Active Motif (Active Motif, Inc.) for the perimenopausal animal model and Vanderbilt Technologies for Advanced Genomics (VANTAGE), Vanderbilt University for the ovariectomy, estradiol prevention and estradiol treatment experiment. Quality control was performed on the RNA samples, and samples with RNA Integrity Index (RIN) > 8 were used for further processing. Enrichment of poly A tailed RNA (m-RNA and some long non coding RNA) and cDNA library preparation was conducted using stranded mRNA (poly A selected) sample prep kit. Sequencing was conducted on Illumina HiSeq 2500 at 50 bp paired-end for the perimenopausal animal model and NovaSeq6000 at 100 bp paired-end for the ovariectomy, estradiol prevention and estradiol treatment experiment. Demultiplexed FASTQ files were developed containing reads on average at 50 million reads/samples for the perimenopausal animal model and 30 million reads/sample for the ovariectomy, estradiol prevention and estradiol treatment samples. The FASTQ files were mapped to cDNA library of the rat genome (Ensemble release 95) to retrieve the count information using Salmon (Patro et al., 2016). To generate counts table from the Salmon output TIxmportV.16.0 was used (Soneson et al., 2015) and DeSEQ2 (Love et al., 2014) was utilized to generate differentially expressed gene list comprised of normalized read counts for each gene/transcript (DEG). Using the normalized counts, inter-sample variability was evaluated by conducting Pearson's correlation in R to identify outliers. Fold changes were established by computing the ratio of the experimental group's average normalized read count versus the control group's average normalized read count. P-values were corrected using the Benjamini and Hochberg False Discovery Rate, total number of significantly DEGs with p-adjusted values less than 0.05 were determined.

Ingenuity pathway analysis (IPA)

IPA was used to conduct discovery-based assessment of the transcriptomic changes between female aging groups. DEG (gene id, p-values, false discovery rate and log expression fold change) files developed from RNA-Seq were uploaded into IPA and only DEGs that had a p-value less than 0.05 were considered for assessment using core analysis. Top canonical pathways and predicted activation and inhibition of upstream regulators generated on the basis of the log expression fold change of the selected genes were used to guide further analysis. Gene lists were defined based on the canonical pathways most pertinent to

the biology of the central nervous system and that have been implicated in the age-related neurodegenerative disorders, especially Alzheimer's disease were investigated(Deczkowska et al., 2018; Heneka et al., 2015; Keren-Shaul et al., 2017; Masuda et al., 2020; Mathys et al., 2017; Von Bernhardi et al., 2015). Comparison analysis was conducted to identify systems most affected by female aging.

Heatmap analysis

Fold changes were computed relative to Reg 6m group and analyzed using heatmap function using Morpheus (https://software.broadinstitute.org/morpheus). For the ovariectomy, estradiol treatment and estradiol prevention, the Sham group was used as the control.

Single tube quantitative Real Time-PCR

To further corroborate findings from the RNA-seq and pathway analysis, single-tube PCR was conducted on select targets. Single-tube PCR was conducted using TaqMan® probes (Thermo Fisher Scientific) for specific targets: MHC-II (*Rt1-Db*: Rn01429350_m1, *Rt1-Da*: Rn01427980_m1, *Rt1-Ba*: Rn01428452_m1, *Rt1-Bb*: Rn01429090_g1). A total of 25 ng of m-RNA was used to convert to c-DNA. Further amplification was done on Applied Biosystems QuantStudio™12K Flex. Ct values generated were converted to ΔCt, on normalization with β- actin Ct values. $\Delta\Delta$Ct values for each sample were generated by normalization with mean values from Reg 6m group. Fold changes with respect to Reg 6m group were generated using $-2^{\Delta\Delta Ct}$.

Tissue sectioning & Immunohistochemistry

Animals were anesthetized after an intraperitoneal injection of ketamine (80 mg/kg) and xylazine (10 mg/kg). Animals were transcardially perfused with phosphobuffered saline (PBS) for 5 minutes and then perfused-fixed with 4% paraformaldehyde (FujiFilm Wako Pure Chemical corporation, cat# 163-20145) for 15-20 minutes, until the peripheral limbs stiffened. A midline incision was made on the cranium and whole brain was harvested from the skull. Meninges were peeled and the brain was immersion fixed in 4% paraformaldehyde overnight, then washed and stored in PBS overnight at 4°C. To cryopreserve the brains were transferred to a 20% sucrose solution (in PBS) for 2 days at 4°C to remove the excess water. The

brains were then stored in PBS at 4°C until sectioned. The brains were embedded in gelatin using the MultiBrain® Technology (Neuroscience Associates, Knoxville, TN) and were coronally sectioned into 40μ thick sections. The sections were immunostained with microglial marker Iba-I (FujiFilm Wako Pure Chemical corporation, cat# 019-19741, 1:500, 4°C, overnight) and reactivity marker MHC-II (Abcam, cat# ab23990, 1:500, 4°C, overnight) followed by secondary antibodies anti-rabbit Alexa Fluor 555 (viewed under Cy3) (Thermo fisher cat# A-21428,1:500, RT, 1 hr) and anti-mouse Alexa Fluor 488 (viewed under FITC)(Thermo fisher cat# A-11001,1:500, RT, 1 hr). Three-dimensional (3D) stacked fluorescent images were taken on Axiovert 200M Marianas Digital Microscopy Workstation, using Intelligent Imaging Innovation, SlideBook6 digital microscopy software (Denver, CO). The images were deconvoluted to the nearest neighbors and a projection was created. Extent of colocalization of the Cy3 and FITC channel was computed using the Pearson's correlation by defining a background region. For the corpus callosum including the cingulum, 7-9 10x images were obtained for each animal. For the Fimbria and Hippocampus CA2 region 3-6 10x images were taken per animal. For each group, average of correlation of the images was computed, and the standard error of mean was computed. P-values were calculated using one-way ANOVA followed by unpaired student t-test. N=3-6 animals/ group.

Adult brain dissociation

Animals of the age 6 month, 9-10 months and12 months were used for primary cell culture and assays. As mentioned earlier, animals from the age groups 6 months and 9-10 months were monitored for reproductive cyclicity for 1 month by vaginal lavages and enrolled into Reg 6m, Reg 9-10m, Irreg 9-10m or Acyc 9-10m groups by the definitions stated above. The 12-month group was not monitored for reproductive cyclicity, as the group was considered reproductively senescent due to age. Euthanasia of the animals was not subjective to the day of cycling in the estrus cycle, to minimize inter-day variability in the functional assays performed. Animals were sedated and the brain was harvested from the skull and kept in ice-cold D-PBS (Gibco™, cat# 14287072). The meninges were peeled off and cortical regions, hippocampi and the white matter were separated on ice. The brain was dissociated using the Miltenyi Biotec adult brain dissociation kit (cat# 130-107-677), using the manufacturer's protocol.

Microglia and astrocyte isolation

Using the MACS Miltenyi Biotec CD11b/c magnetic microbeads (cat# 130-105-634) for rat microglial cells, microglia from the single neural cell suspension generated from the adult brain dissociation kit were magnetically tagged. They were isolated using the manufacturer's protocol. Briefly, separation column was placed in a magnetic field and the magnetically tagged cell suspension was applied to the column. The column was washed and the flow through was collected. The column was removed from the magnetic field, and the microglia were eluted out. The cells collected from the flow through were resuspended in media containing Dulbecco's Modified Eagle Medium/Nutrient Mixture F-12 (DMEM/F-12) (Gibco™, cat# 11039021) and 10% fetal bovine serum (ATCC, cat# 30-2020) and seeded in T25 flask (Thermo Scientific™, cat# 156367) coated with poly-d-lysine (37°C, 2-3 hours) to selectively culture astrocytes. Astrocytes were cultured until 80-90% confluency and were trypsinized and seeded for the metabolic flux assays. Isolated microglia were resuspended in DMEM/F-12 and 10% fetal bovine serum and seeded for metabolic flux assays.

Metabolic flux assays

Using the XFe24 flux analyzer, mitochondrial function was assessed by the measurement of oxygen consumption rate (OCR). Primary microglia and astrocytes cultured from 6-month and 12-month-old animals were seeded in XFe24 cell plates at the densities of 50,000 cells/well and 75,000 cells/well respectively. Assay design and method was developed from studies published in the literature (Irwin et al., 2011a; Irwin et al., 2011b; Orihuela et al., 2016; Sarkar et al., 2017). Microglia were cultured in the plate for 3 days after isolation and, astrocytes for 24 hrs. The day before the assay, the calibration plate was hydrated overnight in a non-CO_2 incubator at 37°C. On the day of the assay, the media was substituted to DMEM (Sigma Aldrich, cat# D5030), which was supplemented with 25mM glucose, 1mM sodium pyruvate and 2mM Glutamine (Gibco™, cat# 25030081). The pH of the medium was adjusted to 7.4 ± 0.05. Following the substitution in medium, the plates were incubated at 37°C in a non-CO_2 incubator for 1 hour. The assay includes baseline measurement of OCR, and serial injections of Oligomycin (1 μM for microglia, 4 μM for astrocytes) (MP Biomedicals, cat# 02151786), FCCP (1 μM for microglia, 2 μM for astrocytes) (Tocris Bioscience, cat# 0453) and rotenone/antimycin (0.5 μM for microglia, 1 μM for astrocytes) (Sigma Aldrich, cat# A-8674). Each injection was followed by the 3 measurements of OCR. This method is used to compute

the baseline respiration, maximal respiration, spare respiratory capacity, ATP production and proton leak. Each assay plate was normalized to protein content to reduce the effect of variances due to cell seeding, cell death or proliferation and a total of 6-8 wells/ group were used.

Measurement of oxidative stress and microglial reactivity

For measurement of microglial oxidative stress and microglial reactivity. MitoSOX™ (Invitrogen™, cat# M36008) staining was conducted by incubating the single cell suspension with 13 μM MitoSOX™ for 10 mins (37°C, non-CO_2 incubator), washed with PBS + 0.5% BSA. The cells were Fc Blocked using Anti-CD32 antibody (BD Pharmingen, cat# 550271) then immunostained with an antibody cocktail: CD11b (Miltenyi Biotec, cat# 130-105-273), CD45 (Miltenyi Biotec, cat# 130-111-774) and MHC-II (Miltenyi Biotec, cat# 130-108-776), for 30 mins on ice. Flow cytometry was conducted on MACSQuant Analyzer 10. Data was analyzed using Flowlogic™V7 (Miltenyi Biotec, cat# 150-000-381). Animals used per group were n =6-8/ group.

Phagocytic capacity assay

For measurement of phagocytic capacity, single cell suspension was incubated with pHrodo™ Red *S. aureus* Bioparticles™ conjugate (Invitrogen™, cat# A10010) at 37°C in a non-CO_2 incubator for 2 hours. Following which, the cell suspension was washed with PBS +0.5% BSA. The cells were immunostained with CD11b (Miltenyi Biotec, cat# 130-105-273), CD45 (Miltenyi Biotec, cat# 130-111-774). The cells were analyzed using MACSQuant Analyzer 10. Data was analyzed using Flowlogic™V7 (Miltenyi Biotec, cat# 150-000-381). Animals used per group were n =4-8/ group.

Gene Expression Omnibus (GEO) dataset analyses

To validate the gene expression data from the perimenopausal animal model, a clinical gene expression GEO dataset GSE11882 was used (Berchtold et al., 2008). Using GEO2R tool, the top 250 gene differentially expressed in the hippocampus were analyzed between 20-34 years (early aging), 35-59 years (mid-aging) and 60 -75 years (late-aging) in females and males (Table S1 & Table S2). Using the early aging group as a sex-matched control, fold changes during mid-aging and late-aging were computed using

GEO2R tool, using default settings, for males and females. Parameters used for analysis are false discovery rate, p-value and log fold change.

Statistical analyses

Statistical analysis was conducted using GraphPad Prism version 8.1. For statistical comparison, one-way ANOVA was conducted unless otherwise mentioned. Correction for multiple test was conducted by Tukey's. For the transcriptomic analyses the statistical comparisons are listed under the RNA-Seq section.

Graphical abstract

Created with BioRender.com.

Supplemental References

Bacon, E.R., Mishra, A., Wang, Y., Desai, M.K., Yin, F., and Brinton, R.D. (2019). Neuroendocrine aging precedes perimenopause and is regulated by DNA methylation. Neurobiology of aging *74*, 213-224.

Barron, A.M., Brown, M.A., Morgan, T.E., and Pike, C.J. (2015). Impact of continuous versus discontinuous progesterone on estradiol regulation of neuron viability and sprouting after entorhinal cortex lesion in female rats. Endocrinology *156*, 1091-1099.

Berchtold, N.C., Cribbs, D.H., Coleman, P.D., Rogers, J., Head, E., Kim, R., Beach, T., Miller, C., Troncoso, J., Trojanowski, J.Q.*, et al.* (2008). Gene expression changes in the course of normal brain aging are sexually dimorphic. Proceedings of the National Academy of Sciences *105*, 15605.

Deczkowska, A., Keren-Shaul, H., Weiner, A., Colonna, M., Schwartz, M., and Amit, I. (2018). Disease-Associated Microglia: A Universal Immune Sensor of Neurodegeneration. Cell *173*, 1073-1081.

Heneka, M.T., Carson, M.J., El Khoury, J., Landreth, G.E., Brosseron, F., Feinstein, D.L., Jacobs, A.H., Wyss-Coray, T., Vitorica, J., Ransohoff, R.M.*, et al.* (2015). Neuroinflammation in Alzheimer's disease. The Lancet Neurology *14*, 388-405.

Irwin, R.W., Wang, J.M., Chen, S., and Brinton, R.D. (2011a). Neuroregenerative mechanisms of allopregnanolone in Alzheimer's disease. Front Endocrinol (Lausanne) *2*, 117.

Irwin, R.W., Yao, J., Ahmed, S.S., Hamilton, R.T., Cadenas, E., and Brinton, R.D. (2011b). Medroxyprogesterone acetate antagonizes estrogen up-regulation of brain mitochondrial function. Endocrinology *152*, 556-567.

Keren-Shaul, H., Spinrad, A., Weiner, A., Matcovitch-Natan, O., Dvir-Szternfeld, R., Ulland, T.K., David, E., Baruch, K., Lara-Astaiso, D., Toth, B.*, et al.* (2017). A Unique Microglia Type Associated with Restricting Development of Alzheimer's Disease. Cell *169*, 1276-1290.e1217.

Love, M.I., Huber, W., and Anders, S. (2014). Moderated estimation of fold change and dispersion for RNA-seq data with DESeq2. Genome Biology *15*, 550.

Mannino, C.A., South, S.M., Inturrisi, C.E., and Quinones-Jenab, V. (2005). Pharmacokinetics and Effects of 17β-Estradiol and Progesterone Implants in Ovariectomized Rats. The Journal of Pain *6*, 809-816.

Masuda, T., Sankowski, R., Staszewski, O., and Prinz, M. (2020). Microglia Heterogeneity in the Single-Cell Era. Cell Reports *30*, 1271-1281.

Mathys, H., Adaikkan, C., Gao, F., Young, J.Z., Manet, E., Hemberg, M., De Jager, P.L., Ransohoff, R.M., Regev, A., and Tsai, L.-H. (2017). Temporal Tracking of Microglia Activation in Neurodegeneration at Single-Cell Resolution. Cell Reports *21*, 366-380.

Orihuela, R., McPherson, C.A., and Harry, G.J. (2016). Microglial M1/M2 polarization and metabolic states. British Journal of Pharmacology *173*, 649-665.

Patro, R., Duggal, G., Love, M.I., Irizarry, R.A., and Kingsford, C. (2016). Salmon provides accurate, fast, and bias-aware transcript expression estimates using dual-phase inference. bioRxiv, 021592.

Sarkar, S., Malovic, E., Harishchandra, D.S., Ghaisas, S., Panicker, N., Charli, A., Palanisamy, B.N., Rokad, D., Jin, H., Anantharam, V.*, et al.* (2017). Mitochondrial impairment in microglia amplifies NLRP3

inflammasome proinflammatory signaling in cell culture and animal models of Parkinson's disease. NPJ Parkinson's disease *3*, 30-30.

Smith, M.S., Freeman, M.E., and Neill, J.D. (1975). The control of progesterone secretion during the estrous cycle and early pseudopregnancy in the rat: prolactin, gonadotropin and steroid levels associated with rescue of the corpus luteum of pseudopregnancy. Endocrinology *96*, 219-226.

Soneson, C., Love, M., and Robinson, M. (2015). Differential analyses for RNA-seq: transcript-level estimates improve gene-level inferences [version 1; peer review: 2 approved]. F1000Research *4*.

Von Bernhardi, R., Cornejo, F., Parada, G., and Eugenin, J. (2015). Role of TGFβ signaling in the pathogenesis of Alzheimer's disease. Frontiers in Cellular Neuroscience *9*, 426.

Wang, Y., Shang, Y., Mishra, A., Bacon, E., Yin, F., and Brinton, R. (2020). Midlife Chronological and Endocrinological Transitions in Brain Metabolism: System Biology Basis for Increased Alzheimer's Risk in Female Brain. Scientific Reports *10*, 8528.

Yin, F., Yao, J., Sancheti, H., Feng, T., Melcangi, R.C., Morgan, T.E., Finch, C.E., Pike, C.J., Mack, W.J., Cadenas, E.*, et al.* (2015). The perimenopausal aging transition in the female rat brain: decline in bioenergetic systems and synaptic plasticity. Neurobiology of aging *36*, 2282-2295.